

2D numerical modelling of soil-nailed structures for seismic improvement

Ali Komak Panah and Sina Majidian*

Faculty of Civil Engineering, Tarbiat Modares University, Tehran, Iran

(Received January 31, 2012, Revised September 30, 2012, Accepted October 09, 2012)

Abstract. An important issue in the design of soil-nailing systems, as long-term retaining walls, is to assess their stability during seismic events. As such, this study is aimed at simulating the dynamic behavior and failure pattern of nailed structures using two series of numerical analyses, namely dynamic time history and pseudo-static. These numerical simulations are performed using the Finite Difference Method (FDM). In order to consider the actual response of a soil-nailed structure, nonlinear soil behaviour, soil-structure interaction effects, bending resistance of structural elements and construction sequences have been considered in the analyses. The obtained results revealed the efficiency of both analysis methods in simulating the seismic failure mechanism. The predicted failure pattern consists of two sliding blocks enclosed by three slip surfaces, whereby the bottom nails act as anchors and the other nails hold a semi-rigid soil mass. Moreover, it was realized that an increase in the length of the lowest nails is the most effective method to improve seismic stability of soil-nailed structures. Therefore, it is recommended to first estimate the nails pattern for static condition with the minimum required static safety factor. Then, the required seismic stability can be obtained through an increase in the length of the lowest nails. Moreover, placement of additional long nails among lowest nails in existing nailed structures can be considered as a simple retrofitting technique in seismic prone areas.

Keywords: pseudo-static; dynamic, seismic improvement; nailing; retrofitting; numerical; finite difference

1. Introduction

In recent years, due to the growing demand for high-rise structures, the use of soil-nailed walls has become increasingly common, particularly as a basement to provide sufficient parking space. The 2003 United State Federal Highway Administration Manual of soil nail walls (Lazarte *et al.* 2003) and the 1999 Japan Railway Technical Research Manual of design and construction of geosynthetic reinforced soil retaining wall (Tateyama 1999) provide design guidelines for soil-nailed structures. However, The main concern of using soil-nailed cuts in high-seismicity regions is the performance of soil-nailed excavations during seismic loading. The post earthquake observations (1989 Loma Prieta, 1995 Kobe, and 2001 Nisqually) indicate that soil-nailed walls appear to have an inherent satisfactory seismic response. This has been attributed to high ductility of nailed structures and possibility of conservatism in the design guidelines (Lazarte *et al.* 2003). Initial studies regarding seismic behaviour of soil-nailed structures were performed after the 1989

*Corresponding author, Ph.D. candidate, E-mail: sina_en412000@yahoo.com

Loma Prieta earthquake in California (Vucetic *et al.* 1998). The post-earthquake observations of nine soil-nailed retaining walls indicated that in spite of high horizontal acceleration, these structures did not show any signs of distress and visible displacements, even though one of them was subjected to horizontal acceleration probably as high as 0.4 g (Vucetic *et al.* 1998). Afterwards, a procedure for dynamic centrifuge testing was developed at UCLA to determine seismic failure mechanism of soil-nailed structures. The results of these studies imply that failure pattern is composed of two sliding blocks and three failure surfaces (Vucetic *et al.* 1993, 1996, Tufenkjian and Vucetic 2000, Kocjan 2005). This mechanism was first referred to as the German type of failure mechanism of soil-nailed walls (Stocker *et al.* 1979). Also, similar failure surfaces were proposed through conducting shaking table tests (Hong *et al.* 2005).

A kinematical pseudo-static working stress analysis approach was developed for seismic design of soil-nailed structures (Choukeir and Juran 1997) on the basis of Juran's working stress method (Juran 1990). This method provides an estimate of the magnitude of the maximum forces mobilized in the nails by assuming a potential slip surface.

Conventional soil nailing design approaches based on limit equilibrium methods fail to address some issues such as soil-nail interaction, nail installation methods, construction sequences and connection between nails and facing. Thus, numerical simulation is normally carried out to investigate complex performance of soil nail walls. Numerical analysis is not only capable of estimating the factor of safety and the stable depth of excavations, but it can also enable computation of values of displacements and mobilized forces in each structural element of nailed slopes during an earthquake. Whereas, the ultimate limit analysis methods can only evaluate the global stability (factor of safety) of excavation. Some researchers have applied two dimensional numerical models for the analysis of nailed soil structures under static conditions (e.g., Shen *et al.* 1981, Cheuk *et al.* 2005, Kim *et al.* 1997, Singh and Babu 2009). In addition, 3-D analyses have been applied to perform more precise numerical simulation (Smith and Su 1997, Zhang *et al.* 1999). However, very few numerical studies have been performed to evaluate the seismic behaviour of soil-nailed structures (e.g., Giri and Sengupta, 2009). Therefore, it seems necessary to perform numerical analysis to study the seismic performance for optimum design of nailing structures.

This study attempts to assess soil-nailed dynamic behavior using 2D Finite Difference Method (FDM) numerical simulation. The numerical simulation was performed through the academic FDM software CA2 (Fakhimi 1998).

2. Model specifications

The two models used in this paper, Models 1 and 2, are 9.6 and 15 meters high and have three and five levels of basement, respectively. The analyzed structures have been selected to be the representative of deep vertical excavations widely used in urban areas. Two-dimensional plane strain models are utilized for the analysis. Due to the 3D geometry of nailed structures with regularly spaced nails, nails and nail-soil interface properties (stiffness and strength) should be divided by the horizontal spacing between nails to average the effect in 3D over the distance between nails for plane-strain simplification (Cheuk *et al.* 2005). The configurations of the numerical models are shown in Fig. 1. Boundary conditions were taken as vertical constraint on the sides of models and full fixity at the base. However, in dynamic time history analysis, free field boundary for the sides and quiet boundary for the below are considered as boundary

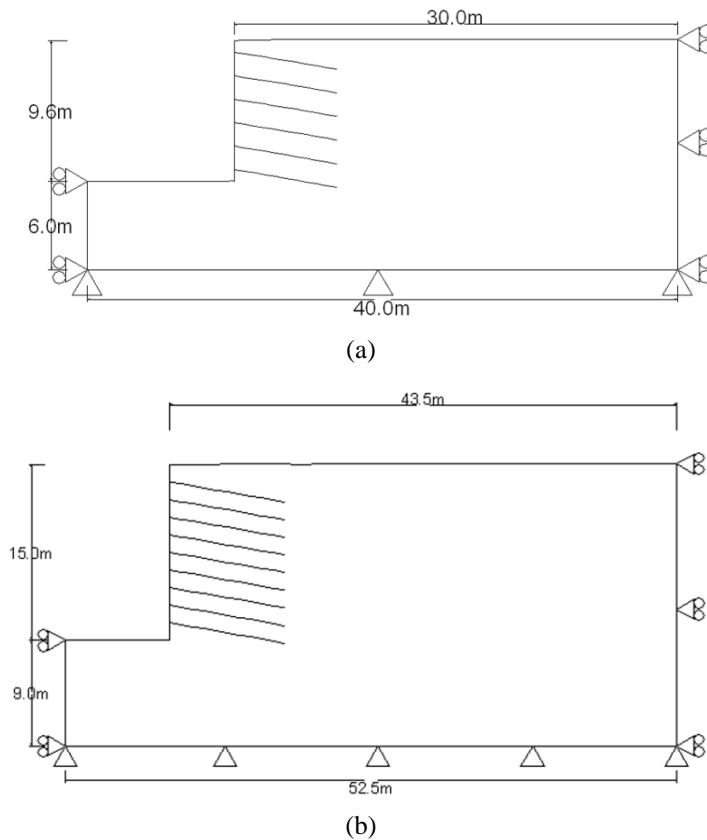


Fig. 1 Models dimensions: (a) Model 1; (b) Model 2

Table 1 Design parameters of nailed structures

	Depth (m)	Soil type	L/H	S_v (m)	S_H (m)	Hole diameter (cm)
Model 1	9.6 m	Nevada 40%	0.72	1.6	1.5	15
Model 2	15 m	Nevada 60%	0.66	1.5	1, 1.5	15

conditions (Fakhimi 1998).

Horizontal and vertical nails spacing (S_v and S_H), nails length and boreholes diameter were considered in a way that the factor of safety of static stability of structures will be remained in the order of 1.35 for both models. These parameters are tabulated in Table 1.

The stages in the construction simulation include successive excavation, erection of nails and shotcreting. The boreholes were drilled by rotary drilled method and grouting was under gravity. The permanent facing is applied after the final lift of the temporary facing (shotcrete with wire mesh as temporary facing) is completed. After permanent lining placement, the effect of temporary facing is ignored. Therefore, after construction stage analysis and prior to dynamic and pseudo-static analyses, placement of permanent facing with high resistance moment was modeled by changing temporary facing parameters.

The soil nails of Model 1 were modeled at a horizontal spacing of 1.5 m. However, the

horizontal spacing for lowest-row nail and other nails of Model 2 were selected to be 1 m and 1.5 m, respectively.

3. Soil parameters

The two models used for simulating soil behavior are described below:

(a) The failure indicator of soil was modeled using the Mohr-Coulomb constitutive criterion. The basic parameters required for modeling are: internal friction angle (φ), dilation angle (ψ) and soil cohesion (C).

(b) The pre failure stress-strain behavior of soil was modeled by the Ohsaki model (Ohsaki 1980) which can predict the nonlinear shear response of soil elements. In deviatoric mode, the nonlinearity in shear and energy dissipation should be considered since soil is likely to experience high shear deformation when a shear wave propagates during seismic motion. Ohsaki model defines the relationship between the second deviatoric invariant stress (J_2) and strain (J'_2) as follow

$$J'_2 = \frac{J_2}{2G_{\max}} \left\{ 1 + \left(\frac{G_{\max}}{100S_U} - 1 \right) \left| \frac{J_2}{S_U} \right| \right\}^B \quad (1)$$

Where, G_{\max} is initial shear modulus, S_u is shear strength and B is material parameter (1.6 for sand and 1.4 for clay). Shear strength can be expressed by Eq. (2).

$$S_U = C \cdot \cos \varphi + \sigma_c \cdot \sin \varphi \quad (2)$$

Where, σ_c is initial confining pressure. It is clear that the number of parameters in the Ohsaki model is less than that in the Mohr-Coulomb model. Furthermore, it is simpler to develop a constitutive law computer code based on Ohsaki model. The Ohsaki model has been applied to simulate soil small strain dynamic behavior in soil-structure interaction problems (Maki and Mutsuyoshi 2004, Nam *et al.* 2006, Maekawa 2003, Tuladhar *et al.* 2008). Combination of the Ohsaki strain-stress model and the Mohr-Coulomb failure criteria has been employed here to model small and large strain soil behavior.

Eq. (1) can be used for initial loading, and unloading and reloading can also determined using Masing rules (Ishihara 1996, Puzrin and Shiran 2000, Muravskii 2001). According to Masing rules, if the loading stress-strain curve follows equation $J_2 = f(J'_2)$ and a reversal stress occurs at a point defined by (J_{2a}, J'_{2a}) , the reloading or unloading stress-strain paths will be determined by equation $\frac{J_2 - J_{2a}}{2} = f(\frac{J'_2 - J'_{2a}}{2})$.

The model presented above has been implemented into FDM code by the writers. In this study, based on experimental data (Alrumoli *et al.* 1992), the properties of Nevada sand with relative densities of 40% and 60% have been used.

The initial shear modulus at different confining pressures can be determined as a function of mean effective stress given by Eq. (3) (Taiebat *et al.* 2007)

$$G = G_0 \left(\frac{p}{p_{at}} \right)^n \quad (3)$$

Where, p_{at} is the atmospheric pressure, G_0 is the shear modulus at atmospheric pressure and n is constant exponent. Initial shear modulus at different depths can be calculated using Eq. (3). Initial values of bulk modulus also can be determined from initial shear modulus and Poisson's ratio using Eq. (4).

$$K = \frac{2.G.(1+\nu)}{3.(1-2.\nu)} \quad (4)$$

Where, Poisson's ratio, ν is estimated using Eq. (5).

$$\nu = \frac{1-\sin\varphi}{2-\sin\varphi} \quad (5)$$

In the Ohsaki model, K remains constant but G changes when an element undergoes shear strain.

Table 2 gives the properties of the Nevada sand with relative density 40% and 60% used in the models.

Fig. 2 shows the shear behavior of Nevada sand with 40% relative density under effective vertical pressure of 80 kPa. The calculated stress-strain behavior when compared to experimental data (Alrumeri *et al.* 1992) is in good agreement.

Table 2 Properties of Nevada sand at relative densities of 40% and 60%

Dr	φ	C	G_0	N	Ψ	ν	γ_{sat}	γ_{dry}
40%	34	0	73 MPa	0.5	0.4	0.31	19.23 kN/m ³	15.07 kN/m ³
60%	36.5	0	85 MPa	0.5	0.4	0.28	19.66 kN/m ³	15.76 kN/m ³

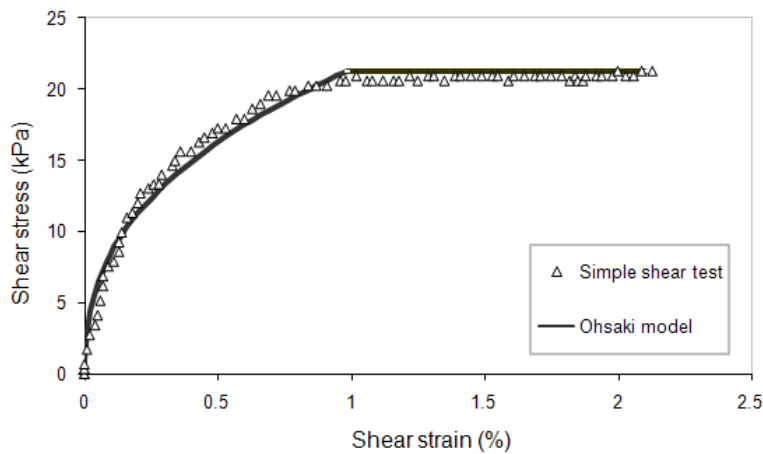


Fig. 2 Simple shear behavior of Nevada sand

4. Structural elements

4.1 Nail

Nails are modeled by elements which are capable of mobilizing axial force and bending moment. Stiffness and strength parameters of steel reinforcement were considered when modeling the nails. Since the grouting was allowed to crack, the grouting stiffness parameters were ignored here.

Nails with diameter of 30 mm and 32 mm; and yield stress of 4000 kg/cm² were used for Models 1 and 2. Nail elements were attached to soil by shear and normal coupling springs simulating soil-grouting interface behavior.

4.2 Facing

The facing was modeled by an element capable of developing plastic hinges.

When internal flexural moment in a facing element reaches its peak value i.e., moment strength, a discontinuity in rotational deflection will develop and additional fictitious nail head axial force will not mobilize. Shotcrete with wire mesh as temporary facing and in situ reinforced concrete as permanent facing were considered in modeling. Moment of inertia, density, Young Modulus and plastic moment of the facing section are the parameters used in analysis. Moreover, bond behavior between soil and facing was modeled using coupling springs.

5. Soil-structure interfaces

5.1 Nail-soil

The interface shear strength between soil and nail is an important parameter for design and stability assessment of the soil-nailed structures. In this paper elasto-plastic tangential spring is used between soil and nail to simulate bond behavior. The strength of shear spring between nail and soil is estimated using the ultimate pullout resistance based on soil type and installation technique (Elias and Juran 1991). Shear spring strength is expressed by Eq. (6) as follows

$$S = \pi \cdot D_b \cdot \tau_{peak} \quad (6)$$

where, S is shear spring strength (N/m), D_b is diameter of borehole (m) and τ_{peak} is ultimate shear stress acting on the bond between grout and soil.

The other elasto-plastic spring parameter which has a prominent role in mobilizing the force in nails is the spring stiffness. A series of laboratory soil nail pullout tests on sandy soils were carried out in the past to investigate the grouted nail and soil interface shear behaviour (Jun 2006, Su *et al.* 2010). In the present study, it is assumed that the peak pullout resistance occurs at pullout displacement within 0.5 cm. This value is in accordance with pullout force-displacement curves presented in previous studies (Jun 2006, Su *et al.* 2010). Thus, spring stiffness shall be determined as follows

$$K_S = \frac{S}{u_p} \quad (7)$$

where K_s is shear spring stiffness (N/m^2), S is shear spring pullout force (N/m) and u_p is pullout displacement at peak pullout force (m).

5.2 Facing-soil

The interface shear behavior between sand and facing has been simulated by an elasto-plastic model. The stiffness value was selected by approximate fitting of hyperbolic sand-concrete model (Gomez *et al.* 2000, 2003). Eq. (8) presents the hyperbolic relation between shear bond stress and sliding

$$\tau = \frac{\Delta_s}{\frac{1}{K_I \cdot \gamma_w \left(\frac{\sigma_n}{p_a} \right)^{n_j}} + \frac{R_f \cdot \Delta_s}{\sigma_n \cdot \tan(\delta)}} \quad (8)$$

Where K_I is dimensionless stiffness value, γ_w is unit weight of water, σ_n is normal stress acting on the interface, p_a is atmospheric pressure, n_j is dimensionless stiffness value exponent, R_f is failure ratio and δ is interface friction angle. The essential parameters were obtained from Gomez *et al.* (2000, 2003).

The shear stiffness which is consistent with the hyperbolic model can be computed utilizing Eq. (9) (Gomez *et al.* 2000, 2003, Green and Elbing 2003).

$$K_s = 0.5 \cdot (1 + R_f)^2 \cdot K_I \cdot \gamma_w \cdot \left(\frac{\sigma_n}{p_a} \right)^{n_j} \quad (9)$$

It can be easily incorporated into the finite difference code. Also, the interface shear strength is estimated by Eq. (10)

$$\tau_{peak} = \sigma_n \cdot \tan(\delta) + C \quad (10)$$

where δ and C are assumed to be $2/3\varphi$ and zero, respectively.

6. Pseudo-static analysis

Pseudo-static analysis involves simulating the ground motion as constant, static horizontal force acting in a direction out of the face of the soil nailed structure. The analysis represents the effects of ground shaking due to earthquake by pseudo-static forces equal to the product of weight of soil mass zones and horizontal seismic coefficient (K_h). In the present study the pseudo-static analysis was carried out by applying the vector sum of the pseudo-static acceleration ($K_h \cdot g$) and gravity acceleration as an artificial gravity field (Fig. 3). The results obtained from the pseudo-static analysis are presented in the form of factor of safety.

7. Dynamic Analysis

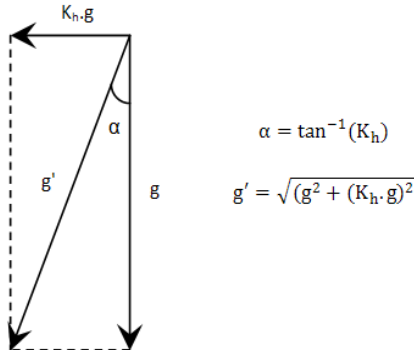


Fig. 3 The vector sum of the pseudo-static acceleration and gravity acceleration

Table 3 The specifications of the test model conducted by Kim *et al.* (1997)

Parameters	Value
Model height	2 m
Soil unit weight	18.2 kN/m ³
Rows of nails	4
Nail length	1.5 m
Nail angle	10°
Internal soil friction angle	39°
Soil cohesion	0 kPa
Young's Modulus of soil	25 MPa
Borehole diameter	6 cm
Nail diameter	1 cm
Nail horizontal and vertical spacing	0.5 m
Peak bond stress strength	34.9 kPa

The dynamic analysis is followed by prescribing the horizontal acceleration time history at the base boundary nodes of the numerical models. The free field boundary conditions are specified along the side boundaries of the models to take account of the wave radiation and minimize the wave reflections. The dynamic analysis capability in CA2 permits two-dimensional nonlinear dynamic analysis. The calculation is based on the explicit finite difference scheme to solve the full equations of motion, using lumped grid point masses derived from the real density of surrounding zone.

8. Verification

In order to verify the modeling procedure, two small scale nailed structures with the following specifications were utilized:

- (a) Kim *et al.* (1997) applied the discrete element method (DEM) to evaluate the stability of reinforced slopes. The proposed approach was evaluated by analyzing the results from a small scale test (Kim *et al.* 1997). In this test model, the mobilized forces in each nail were

measured by load cells installed in front of nails in static loading manner. The specifications of the model are given in Table 3.

Fig. 4 shows the normalized peak axial forces obtained experimentally and derived using numerical simulation. Normalized forces can be determined from Eq. (11)

$$TN = \frac{T_{\max}}{\gamma \cdot h \cdot S_V \cdot S_H} \quad (11)$$

where, TN is normalized peak axial force in the nail length, T_{\max} is peak axial force mobilized, γ is soil unit weight, h is height or depth of structure, and S_H and S_V are horizontal and vertical spacing of nails, respectively.

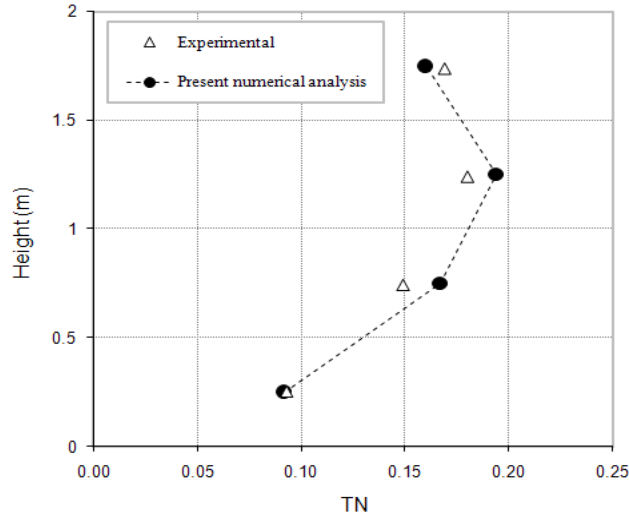


Fig. 4 Normalized experimental and numerical peak axial forces

Table 4 The specifications of the centrifuge model conducted by Tufenkjian and Vucetic (2000)

Parameters	Value
Centrifugal acceleration	50 g
Model excavation depth	152 mm
Prototype excavation depth	7.6 m
Internal soil friction angle	36°
Soil cohesion	7.2 kPa
Young's Modulus of soil	20 MPa
Soil unit weight	15.05 kN/m ³
Rows of nails	3
Nail horizontal and vertical spacing	50 mm
Nail length	102 mm
Cyclic acceleration	0.28 g

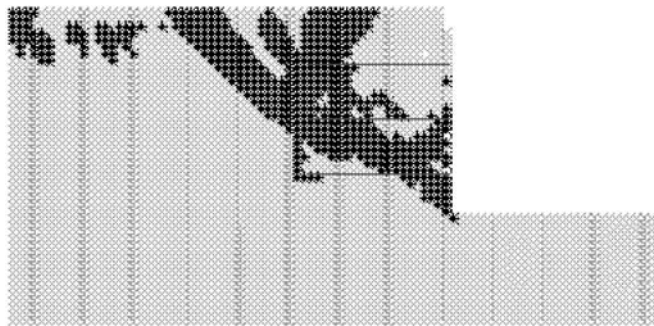


Fig. 5 Plastic regions in centrifuge test simulation

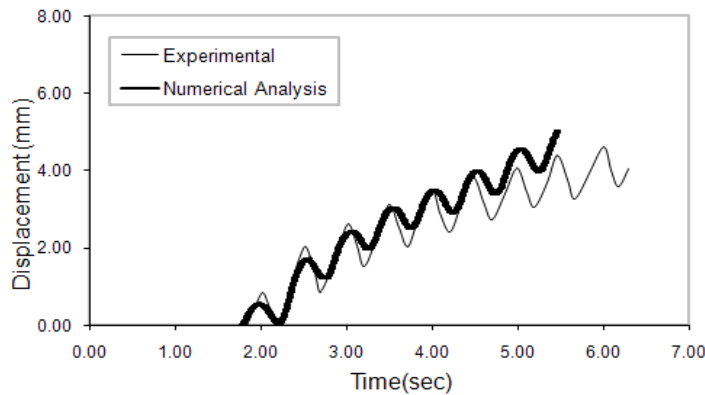


Fig. 6 Horizontal movement of upper nail in experimental test and numerical analysis

- (b) To verify the numerical dynamic model, the centrifuge model (Tufenkjian and Vucetic 2000) has been used. The dynamic centrifuge tests were performed to assess the kinematics and failure mechanism of soil-nailed excavations during strong earthquakes. The specifications of the model are given in Table 4. In this study, the cyclic acceleration with amplitude of 0.28 g was applied for the numerical modeling.

The plastic points are shown in Fig. 5. In a manner similar to results of centrifuge tests conducted by Tufenkjian and Vucetic (2000), three plastic surfaces formed two sliding blocks.

The displacement of facing at the location of the highest nails was measured using displacement transducers. Time histories of the same points were recorded in the numerical models and used for verification. The results of horizontal displacement of the upper nail with time for the experimental test and numerical simulation are presented in Fig. 6.

9. Analysis program

In the current paper, three types of analysis were performed: *construction stage analysis* which simulates excavation, soil-nails installation and shotcreting prior to dynamic analyses; *time history dynamic analysis* which applies 5 cycles of sinusoidal base acceleration at frequency of 3 Hz to the models (if $t < 5/3$, $a_g = \sin(6\pi t)$ and if $t > 5/3$, $a_g = 0$) and *pseudo-static analysis* which simulates

the seismic effects by horizontal forces equal to the product of weight of soil mass zones and horizontal seismic coefficient. In practice, the input seismic forces in the pseudo-static approach are determined by reducing the factor of peak design acceleration. A simple method was used to obtain the seismic coefficient consistent with peak ground acceleration (Komak Panah and Majidian 2010). The maximum cyclic accelerations and seismic coefficients applied to the models are listed in Table 5.

The maximum lateral displacements, development of structural forces and failure modes were studied under both cyclic and pseudo-static loadings so as to evaluate the dynamic performance of soil-nailed walls.

10. Analysis results

When a block of soil is surrounded by plastic (yielded) and excavation surfaces, a sliding block will form and consequently the structure will fail, unless the sliding block is connected to intact soil by elements such as nails. In this paper, first, the failure surface patterns of pseudo-static and dynamic analysis have been investigated. Fig. 7 shows the failure surfaces predicted by dynamic and pseudo-static analysis. As it can be seen, three failure surfaces are formed. In this condition, two sliding blocks, namely reinforced and intact blocks were formed by three failure surfaces. Reinforced soil block is enclosed by a nearly vertical plastic surface behind it. On the other hand, a curved failure surface propagates from the toe into the end of 2nd row nails from bottom. A non-

Table 5 peak cyclic accelerations and seismic coefficients

	Peak cyclic acceleration (g)	0.035	0.1	0.17	0.35	0.5	-
Model 1	Seismic coefficient	0.05	0.11	0.146	0.192	-	-
Model 2	Peak cyclic acceleration (g)	-	0.1	0.17	0.35	0.5	0.6
	Seismic coefficient	0.05	0.11	0.146	0.192	0.238	-

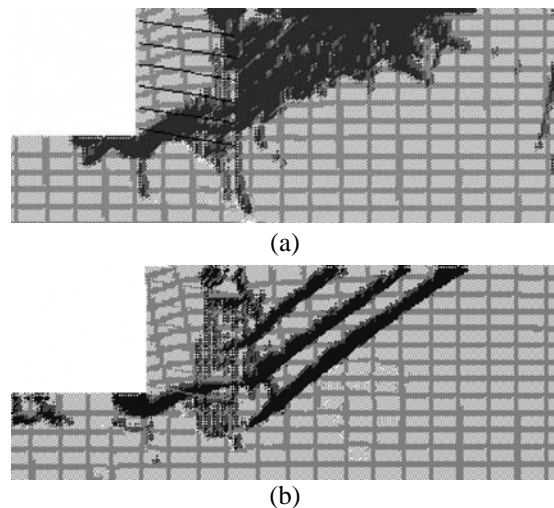


Fig. 7 Dynamic and pseudo-static plastic surfaces: (a) dynamic analysis, (b) pseudo-static analysis

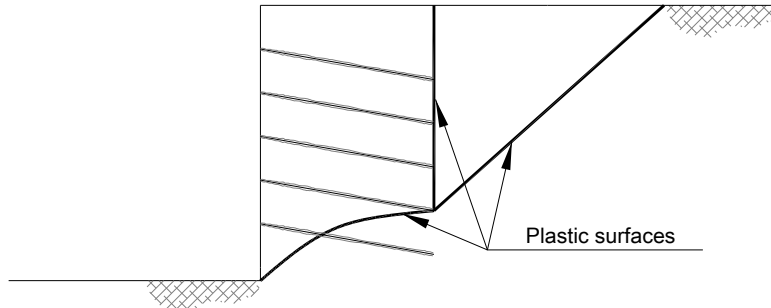


Fig. 8 Schematic plastic surfaces

reinforced triangular wedge which mobilizes the active earth pressure behind the nailed-soil mass is formed by the vertical plastic surface and an inclined slip surface.

This failure pattern is similar to that observed in the centrifuge test (Tufenkjian and Vucetic 2000). However the curved slip surface differs from the linear shape observed in the shaking table test (Hong *et al.* 2005).

Schematic predicted failure pattern is depicted in Fig. 8. In such a mechanism, the bottom nails obviously act as anchors between the back soil and the facing and resist against slope failure.

To confirm this hypothesis, the maximum mobilized forces were determined at the end of construction stage, in the pseudo-static analysis and first cycle of dynamic analysis and plotted against nails depths in Fig. 9. It can be concluded that while cyclic loading has a minor effect on the axial force of upper-row nails, it can cause a significant increase in the axial force of the two or three lowest-row nails. Furthermore, while the models are subjected to strong excitations and pseudo-static forces, the maximum axial forces are mobilized in the bottom-row nails. This implies that the bottom-row nails can act as anchors and inhibit slope failure in the event of strong dynamic and inertial forces when the failure pattern depicted in Fig. 8 is formed.

On the other hand, the numerical simulations revealed that increasing the inertial forces in the pseudo-static analysis and the amplitudes of input cyclic excitation, the plastic surface will enclose all of the soil-nailed mass. This is illustrated in Fig. 10.

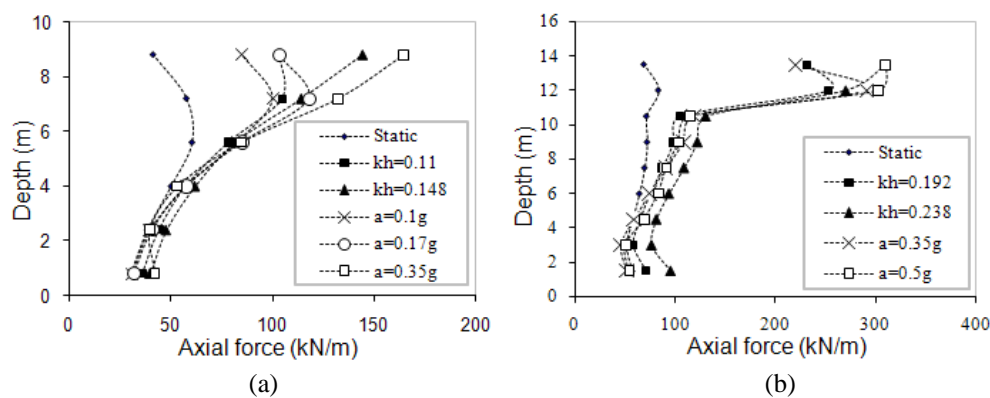


Fig. 9 Maximum mobilized forces in different analyses in: (a) Model 1; (b) Model 2

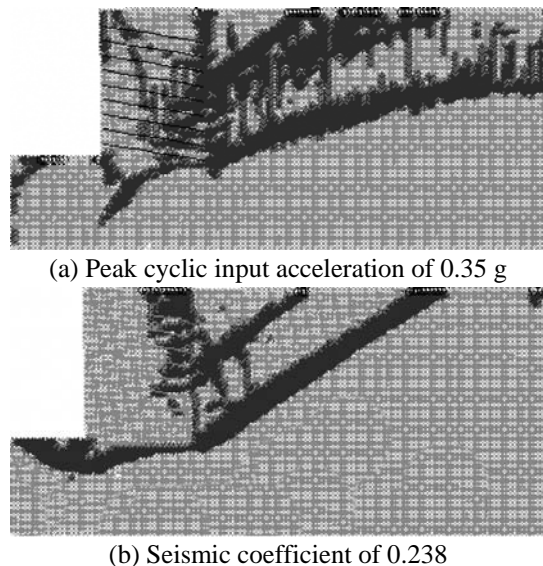


Fig. 10 Dynamic and pseudo-static failure surfaces of Model 2

It is evident that, the bottom-row nails lost their anchoring effect and the structure has failed. Therefore, it seems that the pulling out of nails from the lower rows of nails causes total structure failure. Schematic failure surfaces after pulling out the bottom nails from the intact soil is shown in Fig. 11.

Based on analyses results, Model 1 failure occurs at peak cyclic acceleration between 0.17 g and 0.35 g, and seismic coefficient between 0.148 and 0.192 whereas Model 2 fails at peak cyclic acceleration of about 0.35 g, and seismic coefficient between 0.192 and 0.238.

In the following section, the authors attempt to find a method for increasing the seismic strength by using a larger seismic coefficient or peak amplitude to cause failure of the numerical models.

11. Improvement of seismic strength

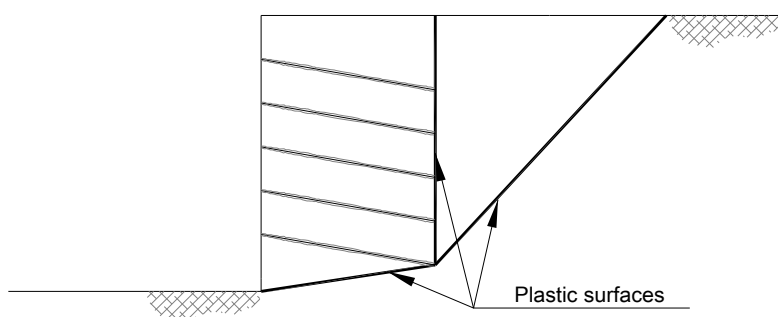


Fig. 11 Schematic failure surface after pulling out the bottom nails

Based on numerical modeling results stated in the previous section, a soil-nailed structure fails when lowest nails lose their anchoring effect and are pulled out from the intact soil region.

Therefore it seems that an increase in the length of the lowest nails would increase the seismic resistance of the slope by increasing the pulling out resistance of the bottom-row nails. To confirm this postulation, a series of additional analyses were performed on models by increasing the length of different nails as shown in Table 6. Behavior of structures under cyclic load and pseudo-static forces due to an increase in the length of the nails is investigated and presented.

Displacement time histories of facing for the initial models and the modified models are assessed. The resulting horizontal movement of points on the intersection of facing and highest row and lowest row of nails for Model 1 and Model 2 are presented in Fig. 12.

As shown in Fig. 12, lengthening the bottom-row nails reduces the translational deformation of the nailed structures subjected to a strong excitation. Meanwhile, the increase in length has no considerable effect on upper point deformation but it reduces the translational motion especially when peak input amplitude is greater than the models failure limits estimated in Section 10.

It can be concluded that the contact point of the bottom nails and facing is the rotational center of facing. Therefore, an increase in the length of bottom row of nails decreases the facing lateral displacement and block sliding and increases seismic stability through reduction of lowest nails pull out but it has no reduction effect on facing rotation. Furthermore, a similar behavior was observed qualitatively in all improved models except Model 2b (the middle nails length have been increased in Model 2b.) in which no considerable change in facing deflection was found in comparison to Model 2.

Table 6 Variation in the length of nails

Models name	Initial nails length	New nails length	Description
Model 1a	7 m	9 m	Lowest nails length increased 2 m
Model 1b	7 m	9 m	Two lowest nails length increased 2 m
Model 1c	7 m	11 m	Lowest nails length increased 4 m
Model 2a	10 m	14 m	Lowest nails length increased 4 m
Model 2b	10 m	12 m	Middle nails length increased 4 m
Model 2c	10 m	12 m	Hole nails length increased 2 m

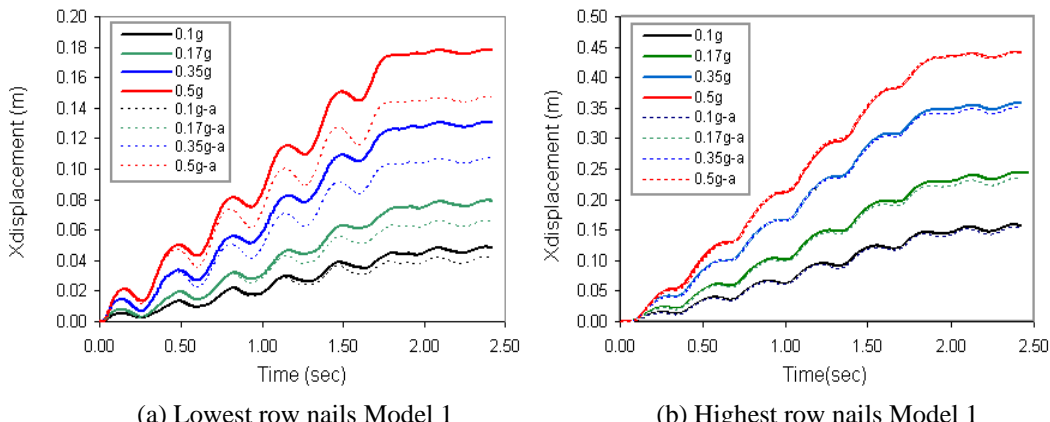
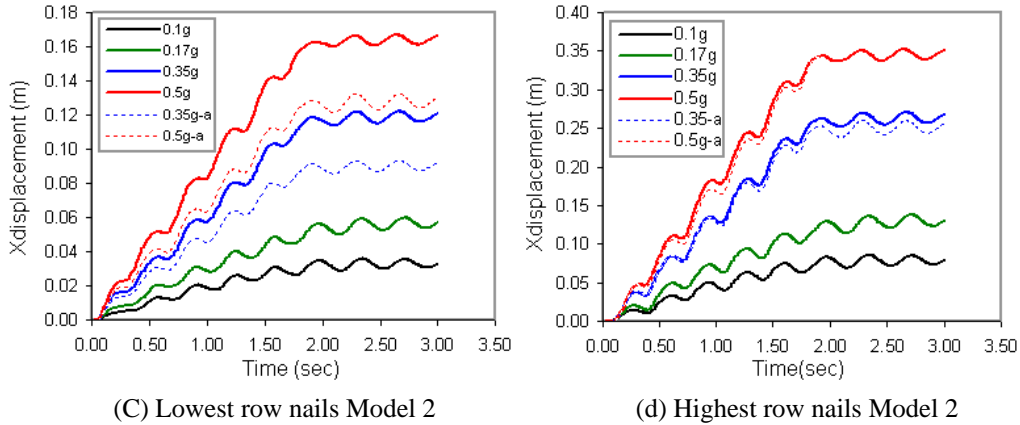


Fig. 12 Continued



(C) Lowest row nails Model 2

(d) Highest row nails Model 2

Fig. 12 Facing displacement time histories

Table 7 Comparison of the maximum facing moment at the location of lowest nails

Models name	$a_{\max} = 0.35 \text{ g}$	$a_{\max} = 0.5 \text{ g}$
Model 1	37 kN.m	38.4 kN.m
Model 1a	42.9 kN.m	43.5 kN.m
Model 2	156 kN.m	162 kN.m
Model 2a	185 kN.m	196 kN.m

It has to be taken into consideration that seismic induced displacements of nailed structures should be computed using design earthquake parameters (e.g., peak acceleration, predominant frequency and duration) and tolerable displacements depend on the service that the wall provides. Design based on the tolerable deformations is found within the framework of performance based design and is beyond the scope of this paper*. In the current research, sinusoidal time history of base acceleration is selected for ease of comparisons.

Another issue that has to be considered is the importance of the facing bending resistance. The results of dynamic analysis revealed that when the models are subjected to strong excitation, the maximum facing moment is mobilized at the location of the lowest nails. In order to show the effect of the proposed method on the development of the bending moment values, Table 7 compares the facing moment at the mentioned location. As can be observed, by increasing the length of the lowest nails, the maximum moment values increase by 13 to 21 percent. When the bending resistance is reached at the facing, no additional head nail force can be mobilized and the soil mass may be pulled out from bottom nails. In other words, longer nails at the bottom do not prevent bending failure of the facing (Kocijan 2005). Therefore, an increase in the length of bottom nails will only be effective if the facing can resist additional mobilized forces.

In order to investigate the seismic improvement of models as a result of increasing the bottom-nails length, factors of safety of the models through pseudo-static analyses are compared. These are listed in Table 8. It should be mentioned that for evaluation of safety factor, both friction angle

*A comprehensive study on performance based design of nailed soil structures is under way by the authors and its outcome will be presented in the future.

Table 8 Factors of safety for considered models subjected to horizontal forces

	$K_h = 0.11$	$K_h = 0.146$	$K_h = 0.192$	$K_h = 0.238$
Model 1	1.09	1.03	0.97	-
Model 1a	-	1.10	1.03	-
Model 1b	-	1.10	1.04	-
Model 1c	-	1.25	1.20	1.09
Model 2	1.26	1.17	1.08	0.98
Model 2a	-	1.27	1.17	1.07
Model 2b	-	1.17	1.08	0.98
Model 2c	-	0.27	1.17	1.08

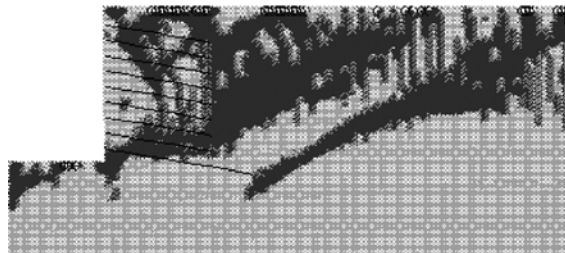


Fig. 13 Dynamic plastic surfaces of Model 2a subjected to peak cyclic acceleration of 0.5 g

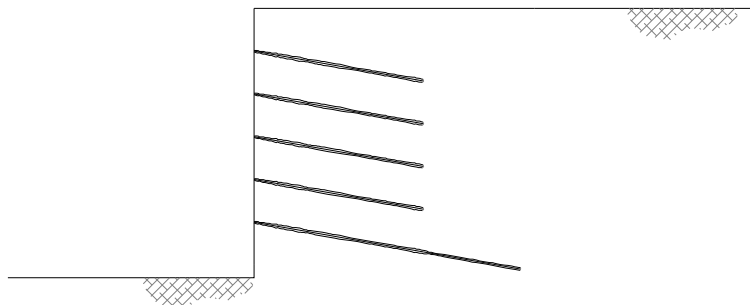


Fig. 14 Schematic nailing pattern suggested for seismic prone regions

and cohesion should be decreased by a constant factor until failure occurs in the model. The least factor which provides a design margin over the design capacity is entitled factor of safety.

By comparing the safety factor values listed in Table 8, the following conclusions are drawn. For a given horizontal seismic coefficient, the models with longer bottom nails have higher safety factors. This means that an increase in the length of lowest nails leads to an increase in the seismic stability of the soil-nailed structure and hence can be used as a method for seismic improvement of nailed structures. Furthermore, it can be postulated that increasing the length of other nails does not have a significant effect on the seismic stability of nailed structures. As shown in Fig. 7, this is justified by existence of an unstable sliding block behind the nails. This block prevents development of anchoring effects in the nails except for the lowest nails. It was obvious that an increase in the length of all the nails will result in larger seismic resistance through the larger shear

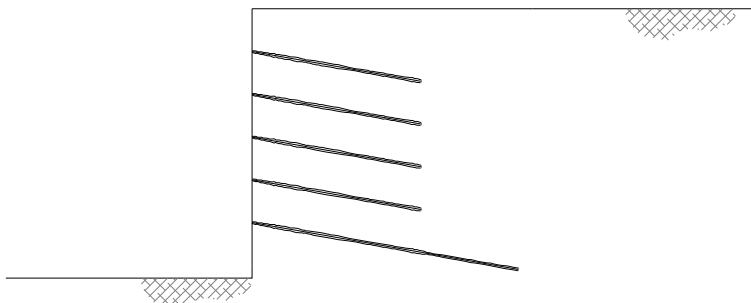


Fig. 14 Schematic nailing pattern suggested for seismic prone regions

strength mobilized in the nearly horizontal lowest plastic surface. However, in comparison with the first method, this method is not economical.

One of the plastic surfaces resulting from improved Model 2a subjected to cyclic acceleration of 0.5 g is illustrated in Fig. 13. It is clear that longer anchoring length of nailed structure subjected to strong excitation prevents the structure to reach the failure mode.

As stated before, a new nailing pattern in which the length of bottom nails is longer than other nails, as shown in Fig. 14, seems to be a proper construction method in high-seismicity regions.

12. Retrifitting of soil-nailed structures

The proposed method is also appropriate for the seismic retrofit of existing grouted nail structures. The strengthening techniques may differ from what is economically available for new construction. In the case of existing soil-nailed structures, placement of additional nails in high depths is not economical. Whereas, placement of additional long nails among lowest nails in existing nailed structures will improve the seismic resistance and can be considered as a simple retrofitting technique for nailed structures vulnerable to seismic actions.

13. Conclusions

The results from this numerical study indicate that three failure surface patterns may form during an earthquake and the lowest row of nails have an anchoring effect and provide the stability for the nailed structures. Furthermore, an increase in the length of lowest nails can be characterized as an effective method to increase the seismic stability of the structure. This is an important aspect of the stability of soil nailed walls that has not been considered yet in the geotechnical practice. Therefore, the authors suggest some design guidelines based on findings in this study. It is recommended to first estimate the nails pattern for static condition with the minimum required static safety factor. Then, the required seismic stability can be obtained through an increase in the length of the lowest nails. However, it is found that increasing the length of the bottom row nails is only effective in improving seismic stability of the structure if the permanent facing can resist the additional mobilized forces.

Acknowledgements

The authors deeply appreciate Professor A. Fakhimi for supplying CA2 for use in this paper.

References

- Alrulmoli, K., Muraleetharan, K. and Hossain M.M. (1992), Fruth LS. VELACS: Verification of Liquefaction Analysis by Centrifuge. Laboratory Testing Program, Soil Data Report, The Earth Technology Corporation, Project NO. 90-0562, Irvine, California.
- Choukeir, M., Juran, I. and Hanna S. (1997), "Seismic design of reinforced-earth and soil-nailed structures", *Ground Improvement*, **1**(4), 223-238.
- Cheuk, C.Y., Ng, C.W.W. and Sun, H.W. (2005), "Numerical experiments of soil nails in loose fill slopes subjected to rainfall infiltration effects", *Comput Geotech.*, **32**(4), 290-303.
- Lazarte, C., Elias, V., Espinoza, R. and Sabatini, P., Geotechnical Engineering Circular No. 7 Soil Nail Walls, *United states Federal Highway Administration*, 1999, No. FHWA0-IF-03-017.
- Elias, V. and Juran, I., Soil Nailing for Stabilization of Highway Slopes and Excavations, *United states Federal Highway Administration*, 1991, No. FHWA-RD-89-193, 199.
- Fakhimi, A. (1998), Theory and user manual of CA2 computer program, Report no. 262, Building and Housing Research Center, Tehran.
- Giri, D. and Sengupta, A. (2009), "Dynamic behavior of small scale nailed soil slopes", *Geotech. Geol. Eng.*, **27**(6), 687-698.
- Gomez, J.E., Filz, G.M. and Elbing, R.M. (2000), Development of an Improved Numerical Model for Concrete-to-Soil Intersection Soil-Structure Interaction Analyses, Report 2, Final Study, ERDC/ITL TR-99-1, US Army Corps of Engineers, Engineer Research and Development Center.
- Gomez, J.E., Filz, G.M. and Elbing, R.M. (2003), "Extended hyperbolic model for sand-to-concrete interfaces", *Geotech. Geoenviron. Eng. ASCE*, **29**(1), 993-1000.
- Green, R.A. and Elbing, R.M. (2003), "Modeling the dynamic response of cantilever earth-retaining walls using FLAC", *Proceeding of the 3rd Int. Symposium on FLAC AND FLAC3D*, Canada.
- Hong, Y., Chen, R., Wu, C. and Chen, J. (2005), "Shaking table test and stability analysis of steep nailed slopes", *Can. Geotech.*, **42**(5), 1264-1279.
- Ishihara, K. (1996), *Soil Behavior in Earthquake Geotechnics*, Clarendon Press, Oxford University.
- Jun, S.L. (2006), Laboratory pull-out testing study on soil nails in compacted decomposed Granite Fill, Ph.D. Thesis, The Hong Kong Polytechnic University.
- Juran, I., Baudrand, G., Farrang, K. and Elias, V. (1990), "Kinematical limit analysis for design of soil-nailed structures", *J. Geotech. Eng.*, **116**(1), 54-72.
- Kim, J.S., Kim, J.Y. and Lee, S.R. (1997), "Analysis of soil nailed earth slope by discrete element method", *Comput. Geotech.*, **20**(1), 1-14.
- Kocijan, J. (2005), Analysis of forces and displacements leading to failure of different configurations of soil-nailed excavation centrifuge models under cyclic loads, Ph.D. Thesis, University of Los Angeles, CA, USA.
- Komak Panah, A. and Majidian, S. (2010), "Assessment of soil-nailed excavations seismic failure under cyclic loading and pseudo-static forces", *Proceeding of the 5th International Conference on Recent Advances in Geotechnical Earthquake Engineering and Soil Dynamics*, San Diego, CA, USA.
- Maekawa, K., Pimanmas, A. and Okamura, H., (2003), *On linear Mechanics of Reinforced Concrete*, Spon Press.
- Maki, T. and Mutsuyoshi, H. (2004), "Seismic behavior of reinforced concrete piles under ground", *J. Advanced Conc. Technol.*, **2**(1), 37-47.
- Muravskii, G. (2001), "Application of experimental results on cyclic deforming of soils to seismic response analysis", *Soil Dyn. Earthquake Eng.*, **21**(8), 661-69.

- Nam, S.H., Song, H.W., Byun K.J. and Maekawa, K. (2006), "Seismic analysis of underground reinforced concrete structures considering elasto-plastic interface element with thickness", *Eng. Struct.*, **28**(8), 1122-1131.
- Ohsaki, Y. (1980), "Some notes on MASING'S law and nonlinear response of soil deposits", *J. Faculty of Eng.*, University of Tokyo, **35**, 513-536.
- Puzrin, A.M. and Shiran, A. (2000), "Effects of constitutive relationship on seismic response of soils, Part I: Constitutive modeling of cyclic behavior of soils", *Soil Dyn. Earthquake Eng.*, **19**(5), 305-318.
- Shen, C.K., Bang, S. and Herrman, L.R. (1981), "Ground movement analysis of earth support system", *J. Geotech. Eng. Division, ASCE*, **107**(12), 1609-24.
- Singh, V.P. and Sivakumar Babu, G.L. (2009), "2D numerical simulation of soil nail walls", *Geotech. Geol. Eng.*, **28**(4), 299-309.
- Smith, I.M. and Su, N. (1997), "Three-dimensional FE analysis of a nailed soil wall curved in plan", *Int. J. Numer. Anal. Method in Geomech.*, **21**(9), 583-597.
- Stocker, M.F., Korber, G.W., Gassler, G. and Gudehus, G. (1979), "Soil Nailing", *International Conference on Reinforce*, Paris.
- Su, L.J., Yin, J.H. and Zhou, W.H. (2010), "Influences of overburden pressure and soil dilation on soil nail pull-out resistance", *Comput. Geotech.*, **37**(4), 555-564.
- Tateyama, M. (1999), Design and Construction of Geosynthetic Reinforced Soil Retaining Wall, *Japan Railway Technical Research*.
- Taiebat, M., Shahir, H. and Pak, A. (2007), "Study of pore pressure variation during liquefaction using two constitutive models for sands", *Soil Dyn. Earthquake Eng.*, **27**(1), 60-72.
- Tufenkjian, M.R. and Vucetic, M. (2000), "Dynamic failure mechanism of soil-nailed excavation models in centrifuge", *J. Geotech. Geoenviron. Eng., ASCE*, **126**(3), 227-235.
- Tuladhar, R., Maki, T. and Mutsuyoshi, H. (2008), "Cyclic behavior of laterally loaded concrete piles embedded into cohesive soil", *Earth. Engng. Struct. Dyn.*, **37**(1), 43-59.
- Vucetic, M., Tufenkjian, M.R., Felio, G.Y., Barrar P. and Chapman, K.R. (1998), Analysis of Soil-Nailed Excavations during the 1989 Loma Prieta Earthquake in California, USGS Professional paper 1552, Part of NEHRP Report to Congress: "The Loma Prieta, California, Earthquake of October 17, 1989".
- Vucetic, M., Tufenkjian, M.R. and Doroudian, M. (1993), "Dynamic centrifuge testing of soil-nailed excavations", *Geotech. Test J.*, **16**(2).
- Vucetic, M., Iskandar, V.E., Doroudian, M. and Luccioni, L. (1996), "Dynamic failure of soil-nailed excavations in centrifuge", *Proceeding of International Symposium on Earth Reinforce*, Fukuoka, Japan, 829-834.
- Zhang, M., Song, E. and Chen, Z.H. (1999), "Ground movement analysis of soil nailing construction by three-dimensional (3-D) finite element modeling (FEM)", *Comput. Geotech.*, **25**, 191-204.